Spatially-Adaptive Reconstruction in Computed Tomography Based on Statistical Learning

Joseph Shtok, Michael Zibulevsky, Member, IEEE,
and Michael Elad, Senior Member, IEEE.

***Abstract*—We propose a direct reconstruction algorithm for Computed Tomography, based on a local fusion of a few preliminary image estimates by means of a non-linear fusion rule. One such rule is based on a signal denoising technique which is spatially adaptive to the unknown local smoothness. Another, more powerful fusion rule, is based on a neural network trained off-line with a high-quality training set of images. Two types of linear reconstruction algorithms for the preliminary images are employed for two different reconstruction tasks. For an entire image reconstruction from full projection data, the proposed scheme uses a sequence of Filtered Back-Projection algorithms with a gradually growing cut-off frequency. To recover a Region Of Interest only from local projections, statistically-trained linear reconstruction algorithms are employed. Numerical experiments display the improvement in reconstruction quality when compared to linear reconstruction algorithms.**

I. Introduction

THE FILTERED Back-Projection (FBP) algorithm is extensively used for image reconstruction in the Computed Tomography (CT). This algorithm implements in the 2-D case a discretization of the inverse Radon transform. Despite the popularity of this method, its drawbacks are non-negligible: FBP fails to account for the numerous physical phenomena present in the data acquisition process (resulting in the well-known streak artifacts) and suffers from discretization errors. Moreover, it lacks the flexibility required to process partial input data, like in the case of projections truncated to a Region Of Interest (ROI), or in the case where projections are restricted to a limited angle range.

Numerous techniques were developed to improve the performance of FBP. Many of them modify the filters, applied to the projection data. The basic problem with the standard Ram-Lak filter [1] is the high-frequency noise amplification. It is commonly treated by using an additional low-pass filter, which cut-off frequency is compatible with the expected bandwidth of the signal. Such an approach requires tuning the cut-off frequency and other parameters of the low-pass filter. The work reported in [2], for instance, is dedicated to tuning these parameters for lesion detectability.

One important task in the clinical CT reconstruction is to recover the CT image in a Region Of Interest in the patient's body using low-exposure scan. To that end, there exist techniques which require projections data only in the neighborhood of the ROI, in addition to a small number of full projections. These techniques employ an FBP modified to compute wavelet coefficients of the sinogram or the sought image by applying wavelet ramp filters [3]–[5]. This allows to recover the high spatial frequencies in the ROI from local data. The low frequencies require full projections; however, since they demand much smaller angular sampling rate, a local reconstruction can be done with much less X-ray exposure. There are, however, no proposed modifications of FBP that undertake the ROI reconstruction in the setup where only projections in the neighborhood of the ROI are measured. Such algorithm would allow further reduction in X-ray dosage, reduce scan duration and dismiss the necessity for the registration of the projection data.

To improve the reconstruction quality and overcome the above drawbacks, statistically-based iterative algorithms were developed. They use an elaborate model for the CT scan measurements, including sources of noise and partial projections data. We refer to [6] for a detailed example of such an algorithm and to [7] for a broad overview of iterative methods. Unfortunately, high computational cost of these algorithms restricts their use in clinical CT scanners.

Superiority of the statistically-based methods stems from the fact the image is reconstructed in a non-linear, locally-adaptive manner, relying only on the available projections data. For instance, with the method described in [6] the reconstruction is performed via optimization of a Penalized Weighted Least Squares (PWLS), with a penalty promoting local smoothness in the image domain in an edge-preserving manner. Such behavior can not be achieved with a linear, spatially-invariant algorithm like FBP. Therefore, an algorithm combining the advantages of both approaches is desired: a direct (and, therefore, fast) processing of the available data, on one hand, with a non-linear, locally-adaptive nature on the other hand.

One such algorithm is developed in [8]. The proposed algorithm uses a powerful filtering technique, involving a training procedure. It employs an exemplar-based classification of the sinogram data patches, combined with training of local 2-D projection filters, which results in a non-linear overall filtering procedure.

In this work we propose a non-linear, locally-adaptive reconstruction scheme, based on example-based statistical learning of its components. The scheme consists of two stages: first, a sequence of linear FBP-like transforms are applied to the available projections data, resulting in a number of preliminary image estimates. Then, a local non-linear fusion

All authors are with the Computer Science Department, Technion - Israel Institute of Technology, Israel.

This research was supported by the European Community's FP7-FET program, SMALL project, under grant agreement no. 225913.

This research was supported by Gurwin Family Fund.

of these estimates is performed to produce the final image.

In the setup of an entire image reconstruction from a full-scan, the linear estimates are obtained with the FBP algorithm with a varying cut-off frequency of the projections filter. A more important goal is to reconstruct an ROI from truncated projections. Since FBP does not perform well in the absence of global projections, we have developed a more flexible linear reconstruction scheme called AFBP [9]. It generalizes the FBP and employs more powerful filters in the sinogram and image domains. The convolution kernels for these filters are derived via statistical training which accounts for missing data and the desired reconstruction properties. In the proposed algorithm, a set of linear estimates of the ROI image are computed by a number of AFBP versions only from projections through a disk containing the ROI, which radius is 110% of the ROI radius. Then the ROI is recovered by a neural network from these preliminary reconstructions by a non-linear, learned fusion rule.

While the computational cost of this procedure is only about ten times the cost of the FBP algorithm[1], two main features distinguish the proposed method from any spatially-invariant reconstruction transform. First, the components of our scheme are designed to work with partial data (truncated projections). Second, the reconstruction is locally adaptive in the image domain, which allows to reduce the noise present in linear estimates and to preserve edges and texture in a better way. The proposed method is labeled as SPADES (SPatially ADaptive EStimator).

This paper extends our work presented earlier in conference publications [9], [10]. Most of the presented material is new, except for the description of the linear AFBP scheme. The SPADES algorithm, which is also briefly presented in [10], has been revised and improved.

The paper begins with Section II, containing preliminaries and notation. For a theoretical motivation of SPADES we present the locally-adaptive denoising algorithm of Lepski, Goldenschluger and Nemirovsky [11] and extend it to CT reconstruction setup (Section III). Then SPADES is described and demonstrated in Section IV. The AFBP scheme is introduced in Section V. Then, the SPADES is extended to ROI setup in Section VI. Discussion follows in Section VII.

II. A model of 2-D Transmission Tomography

A 2-D slice of a physical object is represented by the attenuation map $f(x)$, defined in the domain $\mathcal{A} \subset \mathbb{R}^2$ – this is the image recovered by the CT reconstruction. This map, assumed to have a support radius R, is projected along straight lines by means of the 2-D Radon transform: for $s \in [-R, R]$,$\theta \in [0, \pi]$, the transform $g = \mathbf{R}f$ is defined by

$$g_\theta(s) = \int_{t\in\mathbb{R}} f(s\cdot cos(\theta) - t\cdot sin(\theta), s\cdot sin(\theta) + t\cdot cos(\theta))dt. \tag{1}$$

[1]In practice, the run time can be reduced to one FBP computation by parallel execution on small number of cores.

We denote the range of $\mathbf{R}$ by $\mathcal{P} \subset \mathbb{R}^2$. The adjoint transform $\mathbf{R}^*$, also known as a Back-Projection, is defined by

$$(\mathbf{R}^* g)(x) = \int_\theta g_\theta([cos(\theta), sin(\theta)] \cdot x)d\theta. \tag{2}$$

In the discrete setting, the Radon transform of $f(x)$ is sampled at a large number of fixed angles (evenly covering the range $[0, \pi]$) and fixed signed distances s (bins). The matrix image $f(x)$ is computed from these samples by a discrete reconstruction algorithm.

Let $\ell = \ell(\theta, s)$ be a line which makes the angle $\pi/2-\theta$ with the x axis and passes at a distance s from the origin. To each such line there corresponds a detector which counts the number y_ℓ of photons in a specified time interval during the scan. Due to the limited photon count, the values y_ℓ are modeled as realizations of random variables: $y_\ell \sim$ Poisson $\left(I_0 e^{-(\mathbf{R}f)_\ell}\right)$. The X-ray source intensity I_0 determines the parameters of the Poisson distribution, thus controlling the noise level. The Maximum Likelihood (ML) estimate of $\mathbf{R}f$ from the measurements y_ℓ is $g_\theta(s) = -log(y_\ell/I_0)$. In the ideal case where $y_\ell = \mathbb{E}(Y_\ell) = I_0 e^{-(\mathbf{R}f)_\ell}$ (not attainable in reality since the expectation of Y_ℓ is not, in general, an integer), ML estimate is the true Radon transform of $f(x)$.

More realistic modeling of the CT scan takes into account additional disruptions, such as electronic noise (additive constant in the Poisson parameter λ_ℓ), scatter of X-rays (Compton effect), crosstalk among the detectors, and more [12].

The basic FBP algorithm is defined by means of the linear reconstruction operator $\mathbf{T}_{\text{FBP}} = \mathbf{R}^* \circ \mathbf{F}_{\text{Ram-Lak}}$. Here the filter $\mathbf{F}_{\text{Ram-Lak}}$ is the 1-D convolution kernel, applied to each projection (acolumn in the sinogram matrix). The Ram-Lak kernel ζ is defined in the Fourier domain by $\hat{\zeta}(\omega) = |\omega|$. As mentioned earlier, the Ram-Lak kernel is often smoothed by some low-pass filter compatible to the reconstructed images and the noise level.

III. From Adaptive Denoising Technique to a Fusion Rule for CT Reconstruction

Our goal is to bridge the gap between the linear and the iterative algorithms by a direct reconstruction scheme, locally adaptive to the data. To that end, we employ the technique of filtering with adaptive kernels, developed originally for signal reconstruction from noisy measurements. In the classical setup of the problem, a signal f is measured through

$$y_i = f(x_i) + \xi_i$$

where the set $\{x_i\}$ is a sampling grid and ξ_i are independent normal random variables. The task is to compute an estimate $\tilde{f}(x)$ which minimizes the L_2 norm of the error $\epsilon = |f - \tilde{f}|$ in an interval of interest.

One basic denoising technique is to apply a linear kernel estimator $\tilde{f}_\kappa = y * \kappa$, where κ is a constant convolution kernel representing a low-pass filter. Such an estimator will mistreat those regions where the bandwidth of the signal does not match the bandwidth of the filter (i.e., either the edges will be blurred or the smooth regions will remain noisy).

A substantial improvement can be achieved by using, at each image location, a low-pass filter which cut-off frequency

matches the local spatial smoothness of the signal. Thus, in smooth regions a stronger blur will be used, averaging the noisy values, and near edges almost no blur will be applied in order not to smear them. Of course, such knowledge of the local smoothness of the underlying clean signal is not available, but it can be evaluated using local image statistics. Therefore, given a sequence of filter kernels with gradually growing measure of the blur and a good decision rule, choosing an appropriate filter for each spatial location, a spatially adaptive signal estimator can be implemented.

An analogue of image filtering with kernel κ in CT reconstruction is a linear reconstruction transform $\mathbf{T}$ with the property that the Point Spread Function (PSF) of the (shift-invariant) operator $\mathbf{TR}$ is the kernel κ. It is easy to obtain a sequence $\mathbf{T}_i, i = 1, ..., I$ of linear reconstructors with gradually growing spread of the PSF; therefore an analogue of spatially-adaptive denoising can be designed for CT reconstruction, as we detail in Section III-B. We should stress that the algorithm, described and demonstrated therein, is not intended for practical use: it is a mid-step between the theoretically-based denoising technique for Gaussian noise and the non-linear CT reconstruction algorithm based on a learning machine.

A. Lepski-Goldenshluger-Nemirovsky Estimator

A locally adaptive estimator for signal denoising was devised in the work [11] by A. Goldenshluger and A. Nemirovsky, based on a general scheme by Lepski. Consider again the task of recovering a 1-D signal $f(x)$ from noisy observations $y(x) = f(x) + \xi(x)$ on a discrete grid points $\{x \in \Gamma\}$, where $\{\xi(x)\}_{x\in\Gamma}$ is a sequence of independent normal random variables. To estimate $f(x)$ at some point x_0, a linear combination of the neighboring samples $y(x)$ is taken (as is done by a convolution kernel with corresponding coefficients). The basic idea of this estimator is demonstrated for simple rectangular windows centered in x_0: $\tilde{f}(x_0) = mean\{y(x) \,|x \in \triangle\}$, where $\triangle = [x_0-\delta, x_0+\delta]$. In practice, order-$m$ Least Squares (LS) polynomial is fitted locally into the data.

The error $|\tilde{f}_{\triangle}(x_0) - f(x_0)|$ consists of the deterministic *dynamic error* $\omega_f(x_0, \Delta) = mean_{x\in\triangle}|f(x) - f(x_0)|$ and the *stochastic error* $\zeta(\triangle) = \frac{1}{|\Delta|}\sum_{x\in\triangle}\xi(x)$, introduced by the noise. As the window $\triangle$ grows, the dynamic error increases (with the rate related to the signal smoothness) and the stochastic error decreases, since the noise is averaged over a larger interval. The goal is to find an optimal window width, which balances the error components.

In order to approximate the optimal width, the authors of [11] employ confidence intervals. Consider a sequence $\triangle_1, ..., \triangle_N$ of windows, centered in x_0, with a growing width. For each $\triangle_i$ there is an estimated upper bound ρ_i of the stochastic error in this window. For $i = 1$ it is assumed the the window is small enough so that the dynamic error is dominated by the stochastic one, hence the overall error is bounded from above by $2\rho_1$. The confidence interval related to $\triangle_i$ is then defined by

$$D_i = [\tilde{f}_{\triangle i}(x_0) - 2\rho_i, \tilde{f}_{\triangle i}(x_0) + 2\rho_i]. \tag{3}$$

Notice that for every index i satisfying $\omega_f(x_0, \Delta_i) < \zeta(\triangle_i)$, the total error $|\tilde{f}_{\triangle_i}(x_0) - f(x_0)|$ is smaller than $2\rho_i$ (with the aforementioned high probability). Therefore, the interval D_i contains the true value $f(x_0)$.

In order to estimate the maximal index i^* with this property, the intersection of intervals D_i is considered. A simple argument, presented in [11], shows that if i^+ is the maximal index for which

$$\bigcap_{i<=i^+} D_i \neq \emptyset, \tag{4}$$

then the estimate error is bounded by

$$|\tilde{f}_{i^+}(x_0) - f(x_0)| \leq 6\rho_{i^*} \tag{5}$$

Since the stochastic error ρ_{i^*} is minimal among possible errors corresponding to different segments $\triangle_i$, the choice of $\tilde{f}_{i^+}$ is nearly optimal.

As the simple averaging is replaced with order-m LS approximation, the efficiency becomes comparable to best denoising techniques. It is proven in [11] that such algorithm is near-optimal.

Before passing on to the CT reconstruction, we mention that a similar algorithm was devised by Lepski, Mammen, and Spokoiny in [13]. Both works implement a general scheme of Lepski [14] and seem to share the same approach.

B. A Switch Rule for CT Reconstruction

The denoising technique, described above, requires a preliminary sequence of linear signal estimates, obtained by filtering the noisy signal with a corresponding sequence of convolution kernels (rectangular windows of growing radius, in this case). In the setup of CT, we use a sequence of linear transforms $\{\mathbf{T}_i\}_{i=1}^I$, each is the FBP algorithm involving a low-pass filter with a different cut-off frequency. Let g denote the noisy sinogram and $\tilde{f}_i = \mathbf{T}_i(g)$ is the sequence of image estimates. The the noise, present in the reconstructed images, is of a complicated, data-dependent nature. The denoising algorithm requires to know the bound $\rho_i(p)$ on the statistical error in each image location p of each $\tilde{f}_i$; these bounds can be computed using noise variance in the image domain.

Estimating the noise variance is difficult, and we do not pursue this task here. Our goal is to show that *given the necessary information for the switch rule, locally adaptive CT reconstruction is possible*. Once the evidence for such success is obtained, we propose a different fusion rule, based on a learning machine. Therefore, we simulate a large number on noise instances to compute the variance $\lambda_i(p)$ of the noise at the location p in the image estimate $\tilde{f}_i$. Then, instead of estimating the bound ρ_i on the stochastic error in p as it is done in [11], we compute

$$\rho_i(p) = \kappa(\sqrt{\lambda_i(p)})^q \tag{6}$$

where the parameters κ, q are tuned using a grid search on the training set. These two parameters are required to calibrate the numerical values of the data obtained in CT reconstruction process and are set exactly once for the given setup.

The confidence intervals are computed by the formula 3. Then a switch rule, expressed by the condition (4), is applied to compute the index i^+. The output value in location p is $\tilde{f}_{i^+}(p)$. We label the described algorithm as *LeGoNe* after the authors of the prototypical denoising technique (Lepskii, Goldenshluger, Nemirovski).

C. Numerical Experiment - CT reconstruction with LeGoNe

The quality measure we use is the Signal-to-Noise Ratio (SNR), defined for the true signal f_0 and its estimate $\tilde{f}$ by

$$SNR(f_0, \tilde{f}) = -20log_{10}\frac{\|f_0 - \tilde{f}\|_2}{\|f_0\|_2}. \quad (7)$$

In this experiment we use a set of randomly generated 256×256 geometric phantoms. Each phantom constitute of a large ellipse with boundary and a constant background, filled with many smaller ellipses with randomly chosen centers and radii. There are four intensity levels in each image (also randomly chosen for each phantom). Examples of the phantoms are presented in Figure 1.

Fig. 1: Examples of geometrical phantoms used in the experiments.

In our simulations of CT projection and reconstruction, the projection sets (sinograms) of the reference images are computed using a pixel-driven implementation of a discrete Radon transform $\mathbf{R}$. Its adjoint transform is employed in the reconstruction process. The sinogram noise is generated in accordance to the statistical model, described in Section II (see also the Appendix section for the details).

The sequence of the FBP algorithms $\{\mathbf{S}_i\}_{i=1}^I$ is generated by applying a Butterworth window with growing radius to the Ram-Lak convolution kernel κ_0 in the Fourier domain:

$$\kappa_i = \kappa_0 * \mathbf{F}^{-1}(H_i), \quad H = H(p, q_i) = \frac{1}{1 + q_i^{2p}} \quad (8)$$

Here $\mathbf{F}$ is the 1-D Discrete Fourier Transform. The parameter p controls the steepness of the window roll-off, and q (cut-off frequency) determines its width. $\{q_i\}_{i=1}^I$ is a monotonously decreasing sequence. Figure 2 displays (part of) the corresponding sequence of $\tilde{f}_i = \mathbf{S}_i g$ obtained from a sinogram g of a geometric phantom.

The LeGoNe reconstruction algorithm, as described earlier, is applied using the images $\{\tilde{f}_i\}_{i=1}^I$. Comparison of various reconstruction results can be observed in Figure 3. Notice that, despite the modest increase in the SNR value, much of the noise present in FBP reconstructions is removed in the LeGoNe estimate.

In the switch map generated by the LeGoNe (Figure 4), an intensity value in each location p is the index i^+ chosen for the outcome image in p. It can be observed that in smooth areas of the phantoms the algorithm prefers higher indices (since in blurred images the stochastic error is lower) and near the edges of the ellipses, lower indices are chosen.

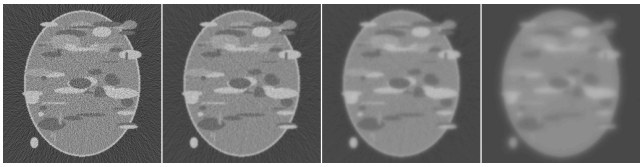

Fig. 2: Sequence of linear FBP estimates for the projected phantom, with a growing degree of blur.

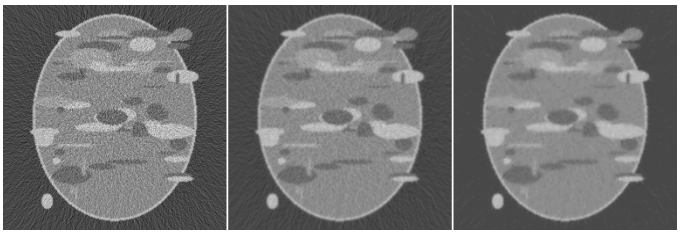

Fig. 3: Reconstruction results, left to right: FBP with ideal Ram-Lak filter, FBP with optimally apodized Ram-Lak filter (SNR = 15.72 dB), LeGoNe (SNR = 16.13 dB).

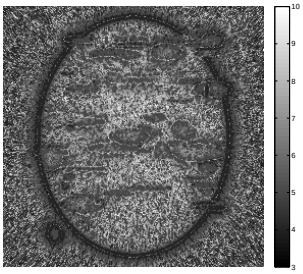

Fig. 4: The switch map of the LeGoNe algorithm.

In practice, the LeGoNe algorithm is not our method of choice. First, the underlying denoising technique is optimal only in the mini-max sense and up to a constant. Second, the evaluation of noise statistics in the image domain is difficult. More importantly, we can not use outputs of other reconstruction algorithms as preliminary results, to be further improved by LeGoNe.

IV. SPADES - Local Fusion Based on a Neural Network

To build a more powerful local fusion rule we resort to a neural network. Indeed, it is difficult to devise an analytical rule to approximate the true image value from the set of preliminary reconstructions $\tilde{f}_i = \mathbf{T}_i g$. The problem is severed by the non-homogeneous, data- and algorithm-dependent noise, present in the image. Yet, by the analogy with the situation discussed in the previous section, we can hope that the set of values $\{v_i = \tilde{f}_i(x)\}_{i=1}^I$, for carefully chosen estimates $\tilde{f}_i$, contains information on $f(x)$ which is more accurate than any of the individual estimates; in other words, there

exists a function $\Psi = \Psi(v_1, ..., v_I)$ that will produce a more accurate image reconstruction when applied point-wise to the set $\{\tilde{f}_i\}_{i=1}^I$.

A neural network can learn this function via a training set of reference images $\{f^t\}_{t=1}^T$ and their simulated estimates $\{\tilde{f}_i^t\}_{1\le i\le I,\ 1\le t\le T}$. The sinogram data is obtained by either applying a Radon transform to discrete reference images, or (in a more realistic setup) by scanning a set of geometric phantoms in a clinical CT scanner. Then the linear reconstruction algorithms are applied in order to compute the training data $\{f_i^t\}$. The learning procedure occurs off-line, and when an unknown object f^n is scanned, the images $\{\tilde{f}_i^n\}_{i=1}^I$ are computed from its projections data and fed to the trained neural network point-wise, to produce the final outcome.

Notice that in this setup we are not confined to use a sequence of linear reconstruction algorithms with a gradually increasing measure of blur, like with the LeGoNe technique. Any available preliminary reconstructions (not necessarily linear) can be fused with the neural network in order to produce a result, expectedly superior to all the participating versions. The scheme of the resulting SPADES algorithm is given in the Figure 5).

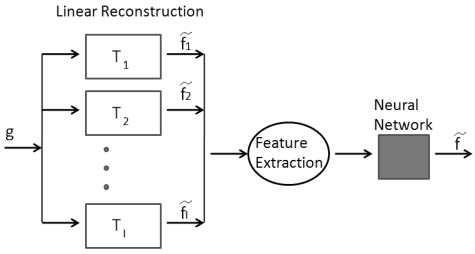

Fig. 5: SPADES reconstruction scheme

A. Algorithm Description

Definition of the neural network: We use a single-layer feedforward type neural network. Its output function is defined by

$$y(x, w, v) = \sum_{j=1}^{N} v_j \sigma(\sum_{k=1}^{K} w_{k,j} x_i + w_{K+1,j}), \qquad (9)$$

where N is the number of neurons, K is the size of the input vector of features x, $w_{k,j}$ is the weight on edge connecting k-th input to j-th neuron and $\sigma(z) = z/(1+|z|)$ is the sigmoid function.

The learning procedure consists in solving the following optimization problem: given a set of vectors of features $x^t = [x_1^t, ..., x_M^t]$ and the corresponding true values $v(t)$ for $t = 1, ..., T$, minimize the objective function

$$(w^*, v^*) = arg \min_{(w,v)} \{\sum_{t=1}^{T} (v(t) - y(x^t, w, v))^2\} \qquad (10)$$

This function is non-convex. In our experiments it is minimized using the Matlab routine *fminunc.m*. It performs an unconstrained optimization using the BFGS Quasi-Newton method with a cubic line search procedure.

Training set design: Notice that intensity values of the reference image $f(p)$ can vary significantly over different regions. We reduce the variability of the data fed to the neural network by using relative values of the images: the vector of features x_p corresponding to a spatial location p is build as follows. The first I values are set to

$$x_p(i) = \tilde{f}_i(p) - \bar{f}(p), \qquad (11)$$

where $\bar{f}$ is the best[2] available estimate of $f(x)$. Other entries of x_p consist of image values in a small neighborhood $\mathcal{N}_p$ of p taken from $\bar{f}$. This provides the neural network with additional local information about the image at the point x, allowing for more accurate restoration of the value $f(x)$.

The corresponding true output value y_p, provided along with the vector x_p in the training stage, is set to $y_p = f(p) - \bar{f}(p)$. In the reconstruction stage, the final outcome image is obtained by

$$\tilde{f}_{nn}(p) = y(x_p, v, w) + \bar{f}(p). \qquad (12)$$

The dynamic range of the input values for the neural network is normalized to $[0, 1]$.

B. Numerical Experiment - SPADES on a full-scan data

We repeat the previous experiment in CT reconstruction, when instead of the LeGoNe switch rule the fusion is performed by a neural network. The training data is extracted in the way described earlier in this section. A network of 24 neurons was trained with a set of 15800 vectors of features (sampled from ten images) and then applied to a test phantom. Ten preliminary versions of each image were built, using an FBP algorithm with varying degree of blur.

The outputs of the FBP and the SPADES algorithms are displayed in Figure 6. It can be observed that the noise streaks, characteristic for FBP reconstruction, do not appear in the SPADES output. It is much closer to the piecewise constant phantom, and the SNR value reflects the quality improvement: it is 2.3 dB higher than the linear reconstruction and 1.8 dB higher than the LeGoNe reconstruction.

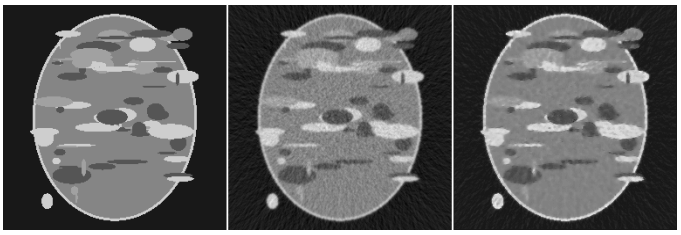

Fig. 6: Left to right: phantom, best linear reconstruction (SNR = 15.72 dB), neural network output (SNR = 18.00 dB)

V. AFBP Reconstruction Algorithm

We describe a design of a linear reconstruction transform, introduced earlier in the conference publication [10].

[2]In the SNR sense. We use the training set to determine which linear estimator is the best.

A. Definition of the AFBP Transform

The extended linear reconstruction operator, labeled as *Adaptive Filtered Back-Projection* (AFBP), is defined in the block diagram given in Figure 7, with parameter set $\kappa = \{\kappa^{\mathcal{P}}, \kappa^{\mathcal{A}}\}$.

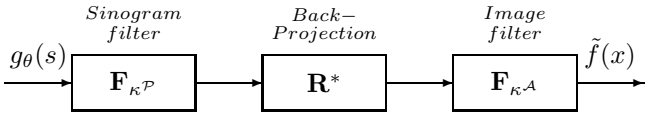

Fig. 7: AFBP reconstruction scheme.

The linear filter $\mathbf{F}_{\kappa^{\mathcal{P}}}$ acts on a sinogram by a distance[3]-dependent 2-D convolution kernel, which definition is detailed below. The filter $\mathbf{F}_{\kappa^{\mathcal{A}}}$ in image domain is implemented as a single 2-D convolution kernel applied to the output of the Back-projection transform.The involved kernels are generated in the training process, described in the SectionV-B.

Filter $\mathbf{F}_{\kappa^{\mathcal{P}}}$ - using 2-D convolution kernels: The ideal inverse Radon operator only requires a 1-D filter applied to each projection. In the practical setup, we use a two-dimensional kernel applied to the sinogram (each projection is also affected by the few neighboring ones). Such a filter exploits the correlation between the neighboring projections and can improve the reconstruction quality.

Filter $\mathbf{F}_{\kappa^{\mathcal{P}}}$ - using a distance-dependent kernel: When the projections are truncated to the ROI, the central part of each remaining projection should be filtered using a symmetric kernel with a small spatial support in order to reduce the truncation error. Near the edges the information should be gathered in a non-symmetric way, only from the non-truncated part of the projection. This can be done by assigning a separate kernel to segments of radial distance from the center of the projection. Explicitly, assume that only projections available are over lines passing through a central disk of radius D in the image domain. We partition the range of distance $s \in [0, D]$ into d disjoint sub-segments $[0, D] = \bigcup_{i=1}^{d} D_i$, and use a bank of $\kappa^{\mathcal{P}} = \{\kappa_i^{\mathcal{P}}\}_{i=1}^{d}$ of corresponding convolution kernels. The filter is applied by convolving the two projection segments corresponding to $\pm D_i$ with the kernel $\kappa_i^{\mathcal{P}}$. See Figure 8 for an illustration.

Here we use the AFBP algorithm in the setup of partial data - truncated projections. This technique also improves FBP performance in the full-scan setup, but in this case the gain is not substantial.

B. AFBP Parameters Training

We state two goals pursued in the parameters training of the AFBP:

Goal 1: Assume availability of a representative set from some family of images, X-ray intensity of the source, radius of a central disk where the projections are measured, and a radius of a central disk where the image should be reconstructed (ROI). The goal is to maximize the reconstruction quality of $\mathbf{T}$, in the Mean Square Error (MSE) sense, for these images

[3]we refer here to the distance s of a projection bin from the center of the projection

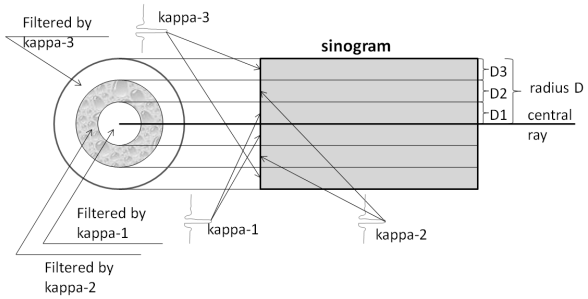

Fig. 8: Illustration of the radially-variant sinogram filtering. In the left part of the diagram: concentric disks in image domain corresponding to horizontal bands in the sinogram.

(the reconstruction is performed from noisy and truncated projections).

Goal 2: Under the same conditions but regardless the X-ray intensity, design a reconstruction operator $\mathbf{T}$ with such that the action of the projection-reconstruction operator $\mathbf{TR}$ will be as close as possible to the action of a radially-symmetric Gaussian convolution kernel in image domain.

The second goal follows from the needs of the non-linear fusion algorithm, which admits at its input a sequence of images reconstructed in different ways. A special case of such sequence, motivated by the LeGoNe denoising technique, is a sequence of images with a growing measure of blur. The AFBP training, corresponding to the stated second goal, will provide us with corresponding sequence of linear operators.

Objective function 1: best image quality. The objective function addressing the first goal is designed as follows. Denote by r the ROI radius. Let $\mathbf{E}_{ROI}$ be the operator which nullifies all the bins in the sinogram matrix which correspond to line integrals outside the central disk (in image domain) of radius $1.1r$. Also, we denote by $\mathbf{F}_{ROI}$ an operator in the image domain that nullifies all the image values outside the ROI.

Given a set $\mathcal{F}_{tr}$ of representative images, we build the training set $\mathcal{G}_{tr}$ consisting of noisy truncated sinograms

$$\mathcal{G}_{tr} = \{g_f^j = \mathbf{E}_{ROI}(\mathbf{R}f + \xi_f^j) \mid f \in \mathcal{F}_{tr},\ j = 1...J\}, \quad (13)$$

where $\{g_f^j\}_{j=1}^{J}$ are obtained from $f \in \mathcal{F}_{tr}$ by applying the Radon transform and generating J instances of Poisson noise. Using this training set, the parameter set κ of the AFBP transform is then computed as an optimizer of the objective function

$$\kappa^* = \arg\min_{\kappa} \sum_{f \in \mathcal{F}_{tr}, j=1...J} \|\mathbf{F}_{ROI}(\mathbf{T}_\kappa g_f^j - f)\|_2^2, \quad (14)$$

where $\mathbf{T}_\kappa$ is defined in previous Subsection.

The objective (14) is quadratic in parameter sets $\kappa^{\mathcal{P}}$ and in $\kappa^{\mathcal{A}}$ separately. Thus, when fixing one, the other is updated by solving a corresponding linear problem (we use the Conjugate Gradients (CG) method). The training is then carried out in turns, fixing one set of variables and updating the other. We do not provide a convergence proof, but the property of the CG

algorithm guarantees a monotonous decrease of the objective function. In practice, we continue the update process until the first 5 significant digits of the objective function are stabilized. In our experience, no noticeable change in the algorithm behavior occurs in case of further optimization.

The resulting linear reconstruction transform $\mathbf{T}_\kappa$ has the following advantages over the conventional FBP:

(1) The objective function adapts the reconstruction operator to partial data conditions, and thanks to its distance-dependent filter such adaptation results in more adequate treatment of the truncated projections.

(2) The adjustment of the low-pas filter parameters in FBP is replaced with automatic derivation of the filter, which cut-off frequency adjusts to the typical spectra of training images and the noise intensity.

(3) The post-processing filter $\mathbf{F}_{\kappa_\mathcal{A}}$ is matched to the projections filter. It helps reducing the value of objective function substantially (as compared to using only projections filter) and therefore to improve the output quality.

(4) The specialization of the reconstruction operator to the given set of images makes it less universal, but improves the reconstruction of similar images. By using a set of images typical to the given task (for instance, sections of CT scans of specific body part), a dedicated reconstruction transforms can be trained for different clinical cases. Another application is to devote a personal reconstructor to an individual patient and use her previous scan data (say, from older similar CT scans) to allow lower X-ray dosage in future scans.

Objective function 2: approximate convolution filter. The objective function built for the second goal involves noiseless projection sets. It has one additional parameter - the standard deviation σ of the Gaussian kernel which action $\mathbf{TR}$ should mimic. The parameter set κ corresponding to the value of σ is computed as the optimizer of the following equation:

$$\kappa^* = \arg\min_{\kappa} \sum_{f \in \mathcal{F}_{tr}} \|(\mathbf{T}_\kappa \mathbf{R} f - \mathbf{F}_{ROI}(\mathbb{G}_\sigma * f))\|_2^2, \qquad (15)$$

This objective function encourages the reconstruction transform $\mathbf{T}$ to produce a blurred output image, which resembles as much as possible the "true" scanned image, filtered with the corresponding Gaussian. Such reconstruction is an alternative to using an FBP algorithm with a low-pass filter applied on the projections. Advantage of the AFBP transform consists in the points mentioned earlier and allows us to use the non-linear fusion in the setup of ROI reconstruction from truncated projections.

Trained kernels: We display visual examples of traned convolution kernels for the sinogram filter of AFBP. in Figure 9 displays two instances of such kernels, one trained for sharp PSF of the $\mathbf{TR}$ operator, and the other one for a wide-spread PSF. The central column of each kernel resemble the Ram-Lak filter, and the neighbor columns (corresponding to neighbor projections) are similar except for the central main peak.The bin values of kernel producing sharp PSF decay rapidly away from the center of the kernel, and the bin values of the blurring kernel are non-decaying, providing input from far projection bins in the convolution process.

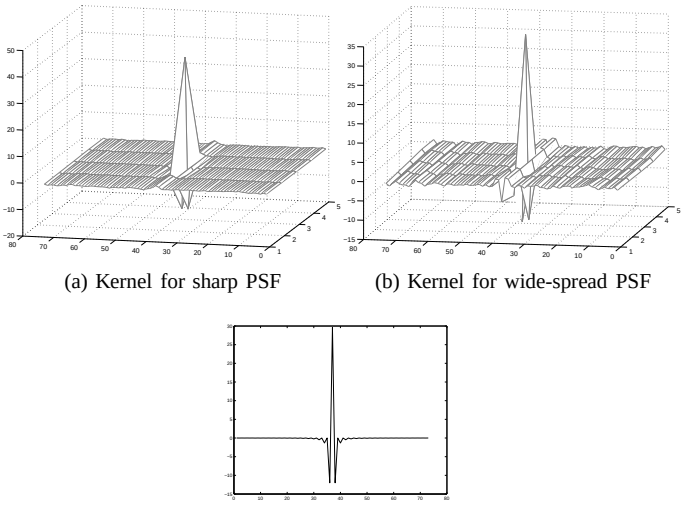

(a) Kernel for sharp PSF (b) Kernel for wide-spread PSF

(c) Ram-Lak kernel

Fig. 9: Bin values of the trained kernels, compared to the 1-D Ram-Lak kernel.

C. Comparison to Previous Work

We return to the previously mentioned work reported in [8]. The Nonlinear Back-Projection (NBP) algorithm, proposed by its authors, employs a different kind of a non-linear filter. It is applied locally to the sinogram data, pre-filtered with the apodized Ram-Lak filter, in the FBP framework. Each small 2-D sinogram patch is filtered by a data-dependent combination of pre-learned filters. The parameters of these filters are statistically trained to yield the lowest MSE values in the image domain for the training set of images. The proposed approach elegantly employs the Gaussian Mixture model in the sinogram domain and its patch-wise classification of the sinogram data has a very good potential to incorporate the sinogram features that would allow high-quality reconstruction.

This technique shares it conceptual approach with the AFBP and the SPADES algorithms, proposed in this article, but can not be directly compared to either one. AFBP also employs a spatially-variant, statistically trained 2-D filter in the sinogram domain, but this filter is linear and not data dependent. SPADES is more closely related to NBP since both algorithms are locally adaptive: NBP employs a sort of data-dependent fusion in the sinogram space, by means of a combination of local filters, and SPADES acts in the image domain, fusing the pre-computed linearly reconstructed images with a neural network. It is difficult to argue in favor of one or the other approach, except maybe for the fact SPADES uses weaker assumptions on the reconstruction problem (we do not assume Gaussian mixture model on small sinogram windows). Unfortunately, we weren't able to conduct a numerical comparison of the two techniques: the results on geometrical phantoms, presented in [8], are inferior to FBP, and the successful experiment on the clinical SPECT data can not be repeated for technical reasons.

D. Numerical Experiments: AFBP on ROI Data

We present numerical experiments of ROI reconstruction from truncated projections. The first one is performed with geometric phantoms, described in Section III. The projections of 15 training images were truncated to a central disk of radius $32+3$ pixels. A Poisson noise, expressed in restriction of the source intensity to $I_0 = 1200$, was applied to the data. The ROI consists of a central disk of radius 32 pixels. The AFBP projections filter is a 2-D radially-variant convolution kernel, as described in Section V-A. Specifically, the size of each 2-D kernel is 5×72 [angles$\times$projection bins], and the ROI radius is divided into 5 sub-segments D_i (overall, 5 2-D kernels). The parameters of the AFBP algorithm were trained using equation (14) and then applied to the truncated, noisy projections of the test image.

For comparison we use the FBP algorithm which is implemented as follows: (1) The Ram-Lak kernel is smoothed by applying a Butterworth apodization window in the frequency domain. The parameters of the window function are tuned on the training set to provide the best SNR value. (2) The truncated projections are extrapolated by replicating the first and the last non-zero rays (see Figure 15). This simple but effective linear sinogram completion technique was described in [5]. See Figures 10,11 for a visual comparison of the algorithms.

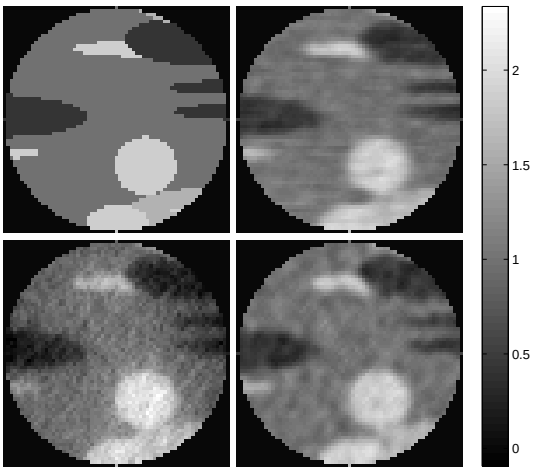

Fig. 10: Reconstruction in a ROI. Upper left: true image, upper right: AFBP reconstruction from truncated projections (SNR = 18.44 dB). Lower left: FBP reconstruction from truncated projections (SNR = 14.55 dB). Lower right: FBP reconstruction from full data (SNR = 18.06 dB).

The experiment was repeated on a set of clinical CT images, which represent axial head sections (courtesy of the *Visible Human* project[4]) The CT scan was performed on a GE scanner and consists originally of 512×512 grayscale images with pixel depth of 12 bits. The images were cropped and resized to 256×256 size for the purpose of our experiments. Some of them are displayed at Figure 12). Figure 13 displays the ROI and a typical result of reconstruction from truncated projections. In Figure 14 we compare the AFBP versus the FBP algorithm.

Fig. 11: Error images $|f_{orig} - \tilde{f}|$ in the ROI. Left to right: AFBP on truncated projections, FBP on truncated projections, FBP on full data. Darker shades correspond to larger error.

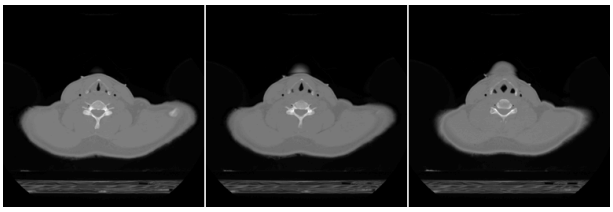

Fig. 12: Clinical CT images from the AFBPt training set

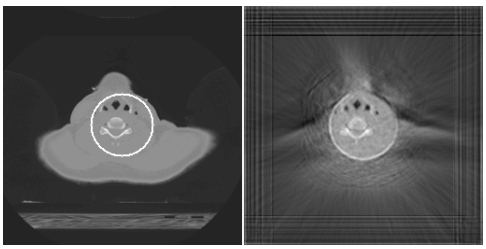

Fig. 13: Left: true image with a marked Region Of Interest. Right: full reconstruction from truncated projections by AFBP. The ROI is clearly distinguished.

It can be seen from the images that AFBP improves substantially the FBP output, producing an image comparable to a reconstruction from full scan data. The SNR values support this observation.

E. Study of AFBP and FBP Algorithms on ROI

We now turn to second kind of AFBP transforms $\mathbf{T}_i$, trained by optimizing the equation (15) for different values of σ_i. These reconstruction transforms come to replace a sequence of FBP transforms $\{\mathbf{S}_i\}_{i=1}^{I}$ in ROI reconstruction, due to the need to adjust the linear reconstructors to the missing data setup: FBP is theoretically derived for full-data scan and its performance of truncated projections is poor, even with optimized parameters of the low-pass window[5].

Now we define a measure on a reconstruction transform $\mathbf{X}$ that expresses the amount of blur $\mathbf{X}$ introduces into the output image. Let $\mathbb{G}_\sigma$ stand for the rotationally symmetric 2-D Gaussian convolution kernel with standard deviation σ.

[4]www.nlm.nih.gov/research/visible/visible_human.html

[5]which indeed make a significant difference in FBP performance.

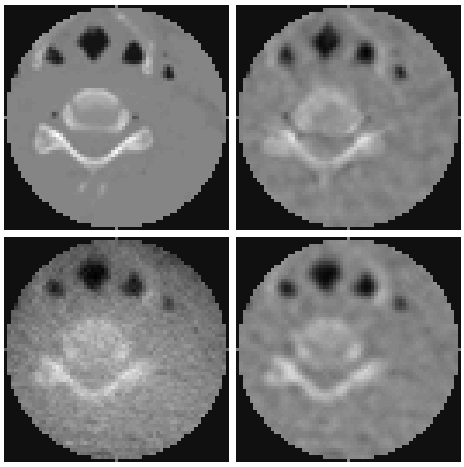

Fig. 14: Reconstruction in a ROI. Upper left: true image, upper right: AFBP on truncated projections (SNR = 22.05 dB). Lower left: FBP on truncated projections (SNR = 15.73 dB). Lower right: FBP on full data (SNR = 22.28 dB).

Given a training set $\mathcal{F}_{tr} = \{f_1, f_2, ..., f_N\}$, we define

$$\zeta_{\mathbf{X}} = arg\min_{\sigma} = \frac{1}{N}\sum_{j=1}^{N} \|\mathbf{X}\mathbf{R}f_j - \mathbb{G}_\sigma * f_j\|_2 \qquad (16)$$

In words, the *blur measure* $\zeta_{\mathbf{X}}$ is the standard deviation of a Gaussian kernel which action on images of the training set resembles the most (in MSE sense) the action of $\mathbf{XR}$. Notice that the value of $\zeta_{\mathbf{X}}$ is, up to a constant, the Full-Width-Half-Maximum (FWHM) of the effective Gaussian blurring kernel, since the FWHM of a Gaussian is 2.35 multiplied by its standard deviation.

Notice that for the AFBP transform $\mathbf{T}$ trained via equation (15) with corresponding standard deviation σ_T, we have $\zeta_{\mathbf{T}} = \sigma_T$. For any other transform $\mathbf{X}$ the blur measure can be easily approximated by evaluating the optimizer of (16) via a grid search on values of σ.

The blur measure will allow us to parameterize the sequences $\{\mathbf{T}_i\}, \{\mathbf{S}_i\}$ of reconstruction algorithms in order to correctly compare their performance: for a given level of noise present in the sinogram, the output quality is a function of the blur measure applied in the reconstruction process.

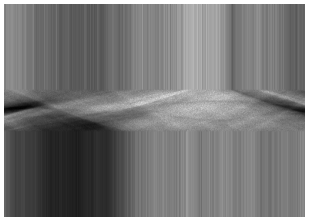

Fig. 15: Sinogram completion method used for FBP. The horizontal band in the middle of the image represent the available projections, truncated to the central disc in image domain. Other rows are replica of the upper and lower margins of the band. This simple step helps improving the FBP performance substantially.

More importantly, this notion allows us to unambiguously characterize the sequence of reconstructors, employed in the first stage of the SPADES algorithm, instead of specifying the parameters of apodization window for FBP or the values of σ_i for AFBP.

In the following numerical experiment, a sequence $\{\mathbf{T}_i\}_i$ was trained on 15 geometric phantoms by optimizing the equation15, in the setup described in the beginning of the Section V-D. Using these phantoms, the values $\zeta_{\mathbf{T}_i}$ are computed empirically, as well as the values of $\zeta_{\mathbf{S}_j}$ for FBP transforms with corresponding cut-off frequency q_j (see equation (8)). We used different values of the parameter p, to achieve best available quality for the FBP. All algorithms are applied to noisy truncated projections, mended by the aforementioned completion technique (see Figure 15). In Figure 16 we present graphs of SNR values of phantoms reconstructed from noisy and truncated projections, with the same setup as in the previous experiment. Specifically, we plot average SNR values over a set of phantoms, as function of the blur measure. The comparison is carried out between the AFBP and the apodized FBP with different values of p. It can be seen that with $p = 0.5$, FBP achieves maximal quality at $\zeta \sim 2.1$, which is substantially lower than SNR values achieved by the trained kernel of AFBP at $\zeta \sim 1.2$.

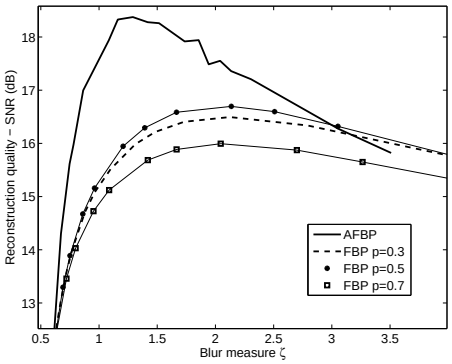

Fig. 16: Graphs of reconstruction quality versus the blur measure $\zeta_{\mathbf{T}}$, computed for the sequence of AFBP transforms and also for three sequences of apodized FBP transforms with different degrees p of Butterworth window.

VI. SPADES IN THE ROI

A. The Algorithm

We return to the SPADES algorithm (see Section IV) with AFBP transforms. Now it can be extended to the setup of ROI reconstruction from truncated projections. To that end, AFBP transforms of two types, corresponding to objective functions (14),(15) are used:

(1) One transform $\mathbf{T}_o$, trained with (14), will produce an image of best quality (in SNR terms) attainable with AFBP at the given noise level, for images similar to those of the training set.

(2) A sequence of transforms $\{\mathbf{T}_i\}_{i=1}^{I}$ trained via the equation (15), will produce a set of image versions with a growing blur, corresponding to standard deviation values $\{\sigma_i\}_{i=1}^{I}\}$. we use $I = 10$ such transforms.

The training of AFBP versions is performed on a given set of images. Afterwards, the same training set is used to compute the weights of the neural network, while the inputs are obtained from the linear AFBP image estimates. When all components of the SPADES reconstruction are ready, the processing of the sinogram data g_n for an unknown image is carried out in three steps (see a diagram in the Figure 5):

1) Compute preliminary images $\tilde{f}_i = \mathbf{T}_i g_n, i = 1, 2, ..., I$, and $\tilde{f}_o = \mathbf{T}_o g_n$.
2) For each pixel p in the ROI, build a vector x_p of features from the corresponding values of $\tilde{f}_i, \tilde{f}_o$ (see Section IV-A for details).
3) Use the neural network to compute the value of the output image at p from the vector of features x_p.

B. Computational Complexity of SPADES

The computational complexity is calculated for images of size $n \times n$ and for $I + 1$ preliminary reconstruction operators.

(1) The standard FBP algorithm, which consists of a 1-D filtering of the sinogram columns and a Back-Projection transform, requires $\mathbb{O}(n^3)$ computations for each of these steps. The AFBP differs in the $2 - D$ sinogram filter, which uses about $3 - 5$ times more operations than a $1 - D$ filter, and in a 2-D post-processing filter which consumes $\mathbb{O}(n^3)$ computations: we used a $2-D$ kernel of dimensions $\sqrt{n}\times\sqrt{n}$, therefore its action requires n operations per pixel. Therefore AFBP has the overall complexity of $\mathbb{O}(n^3)$ computations.

(2) SPADES involves $I+1$ versions of the AFBP transform. If the computing machinery allows to execute the $I+1$ AFBP algorithms in parallel, time consumption of the preliminary stage equals to a single FBP reconstruction. Otherwise, the preliminary step requires $\mathbb{O}(I \cdot n^3)$ operations. Typical value of I, used in our experiments, is $I = 10$.

(3) The neural network involves $(I + 11)N$ weights, which participate in the computation of every pixel in the image. Here N is a number of neurons and (again, in our experieece) it should be roughly equal to the size of the vector of features, $I+10$. Thus, computation of each intensity value for the output image requires $\sim\ (I + 10)^2 \sim 400$ operations.

(4) If the number of pixels in ROI is M, the overall complexity is $\mathbb{O}((I+1)n^3+(I+10)^2M) \sim \mathbb{O}(10n^3+400M)$ operations.

C. Numerical Experiments - SPADES on the ROI data

In the first numerical experiment, we used a training set of 15 geometric phantoms, described earlier. The chosen blur measure values $\zeta_{\mathbf{T}_i}$ are equally spaced in the interval $[0, 3.5]$. Linear reconstruction of the ROI in a test image with AFBP algorithms was conducted from noisy and truncated projections (see experiment setup in Section V-D. The neural network was applied on the resulting images to produce the final output.

Outcomes of three different algorithms are visually compared in Figure 17: a linear reconstruction scheme AFBP, a locally-adaptive direct algorithm SPADES and a statistically based iterative algorithm [6] (see the Appendix section for details of our implementation). It can be observed that SPADES has succeeded in reducing the background noise, stemming from low X-ray intensity, restoring the piece-wise constant texture of the phantom. The SNR value of SPADES output is higher by 1.15 dB than the SNR of best linear algorithm output we could produce. The statistical reconstruction result has sharper edges and more homogeneous ellipses, at the price of higher computational time. Notice that because of artifacts its SNR value is still lower than that of SPADES output. The reconstruction was further carried out on 23 other test images. The average SNR values of the ROI quality are: FBP (on truncated projections) - 15.80 dB, FBP (on full data) - 18.89 dB, AFBP (on truncated projections) - 19.31 dB, SPADES (on truncated projections) - 20.30 dB. Such quality improvement was possible due to the fact FBP displays discretization artifacts, which restrict the reconstruction quality even in the absence of noise and with no truncation of the projections. The learned kernels of AFBP succeed to partially compensate this drawback.

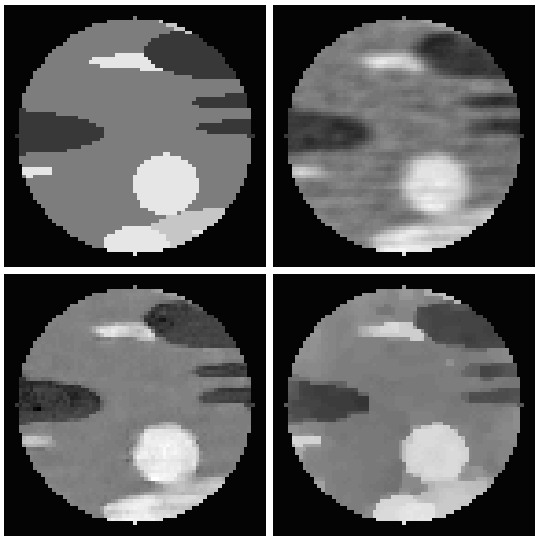

Fig. 17: Upper left: true image. Upper right: best AFBP version (18.44 dB). Lower left: SPADES reconstruction (19.81 dB). Lower left: Statistical reconstruction (19 dB).

The experiment was repeated for a ROI reconstruction in the Forbild head phantom, designed in the framework of the Forbild project [6]. A set of ten similar phantoms, obtained from the head phantom by random perturbations of the radii and locations of the composing ellipses, served as a training set for SPADES. The behavior of the involved algorithms (AFBP, SPADES and the statistical reconstruction) was similar to one observed in the Figure 17. Numerically, the quality of ROI recovered by AFBP in the Forbild phantom was 17.93 dB, statistical reconstruction has achieved the same value, and SPADES has demonstrated 20.1 dB. Due to the lack of space, we omit the accompanying graphics.

Another experiment was carried out with the clinical CT images, described earlier in the Section V-D. The AFBP output, generated in the earlier experiment on CT data (Section V-D, Figure 14), is used, along with a sequence of blurred

[6] http://www.imp.uni-erlangen.de/forbild/english/results/head/head.html.

versions of the test image, as the input data for the neural network. The parameters of AFBP , as well as the neural network, were trained using a set of 10 clinical images (some are presented in Figure 12). Output of AFBP, SPADES and the statistical algorithm are displayed in Figure 18. Their behavior is similar to the one observed on the phantoms. The linear AFBP produced a good[7] preliminary image, which nevertheless contains noise propagated from the projections. SPADES succeeds to remove the noise substantially, resulting in an image close to the ground truth. The statistical algorithm also produces a clean image, but the artifacts introduced by the Huber prior deteriorate its quality. SNR values reflect on these observations.

In the reconstruction of 16 additional test images, average SNR gain of the SPADES algorithm over the AFBP was 1.93 dB. This shows consistency in the behavior of the two algorithms, visually displayed in the Figure 18.

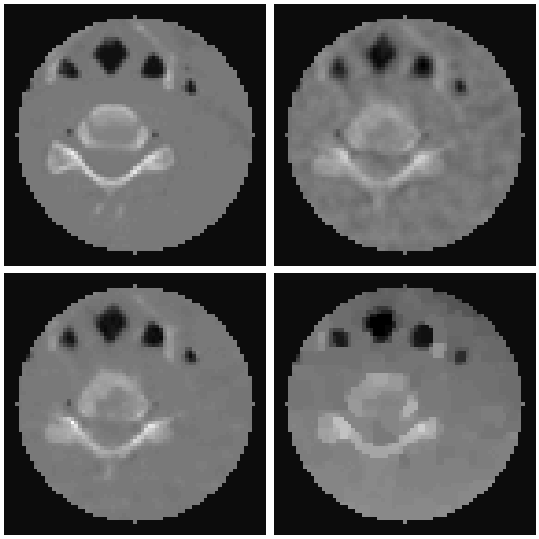

Fig. 18: Upper left: true image. Upper right: best linear AFBP (22.04 dB). Lower left: SPADES reconstruction (24.58 dB). Lower left: Statistical reconstruction (19.24 dB)

VII. Discussion and Conclusions

We have proposed and demonstrated a CT reconstruction algorithm based on a local fusion of linear estimates of the sought image. The linear reconstructors were designed to automatically adapt to the specific family of images and the noise level, as well as the missing data setup. Resulting direct non-linear reconstruction algorithm produces images inherently different from those obtained with FBP or other linear methods: the noise level and artifacts are substantially reduced, while the edges present in the image are well preserved. We notice that the proposed method can in principle improve any given reconstruction method, by fusing its output image with a number of other image estimates by an adequately trained neural network.

The proposed scheme involves very few parameters, mostly the design details - number of linear reconstructors and their blur measure values, structure of the vector of features and number of neurons. All these are easily tuned in a practical setup of specific implementation of the algorithm. Admittedly, the neural network requires a delicate treatment, but in our experience (and especially for specialists in Machine Learning) it is fairly manageable. In fact, we used the simplest one-level feed-forward model of the neural network, and it is plausible that using more complex network (with larger training set) will improve the algorithm behavior.

We notice that the proposed scheme performs an isotropic processing in the image domain: the inputs of the neural network are preliminary images $\tilde{f}_i = \mathbf{TR}f$ which approximate the true image $f(x)$ convolved with a *radially symmetric* kernel. The FBP algorithm also has a radially symmetric PSF. A promising future direction of work is an extension of SPADES to an anisotropic algorithm, where elliptical kernels with varying directions and dimensions are used. The neural network should automatically choose the relevant direction (or combination of some), to use the appropriate preliminary image version at each point

All the numerical results presented in this paper were obtained from experiments executed entirely in the Matlab environment. The "ground truth" images are projected using one specific implementation of the discrete Radon transform, and also used as the ideal reference for the training purposes. Admittedly, the results are affected by this setup, hence the experiments should be rendered as synthetic. The proposed methods can be extended to a practical setup by using mechanical phantoms with geometric details and their discrete computerized models. Despite the absence of realistic clinical data experiments and industrial implementations of the FBP in the experiments, the differences observed between the existing and the proposed techniques are consistent and explicit. Therefore, we hope that presented techniques will also exhibit similar behavior when applied in the industrial CT setup.

Notice that incorporating the proposed algorithm into an existing CT machinery will only require minor software modifications - replacement of FBP filters and addition of a learning machine. Since SPADES is not slower than the standard FBP algorithm (when parallel computation of FBP instances is available), it represents an appealing alternative for full-scan reconstruction and especially for ROI recovery from partial data.

In a broader view of numerical algorithms for inverse problems, the proposed technique has quite a general underlying principle: a fusion of a sequence of solutions with a certain structure, using a discriminatively trained learning machine. One possible application of this principle can be considered for the very common method of solving an inverse problem by optimization of the objective function of form

$$x^* = arg\min_x \{D(x,y) + \lambda P(x)\}. \qquad (17)$$

Here y is a set of measurements, x is the sought signal, $D(x,y)$ is the Data component which encourages the consistency of the solution with the observations and $P(x)$ is a Prior component, expressing the beliefs on the nature of the signal x. The optimizer is usually obtained by an iterative update of the

[7] see section V-D for comparison with FBP

initial solution x_0. The parameters of the algorithm, such as the value of λ and the number of iterations, are crucial for successful reconstruction but are difficult to estimate and often are data-dependent.

An appealing solution to the problem of chosing the parameters would be to compute a set of optimizers x_i^*, corresponding to different values of λ and/or the number of iterations. These preliminary optimizers would then be fused into the final output by means of a neural network (or other learning machine), trained on samples from a training set. Such approach (on expense of higher computational complexity) is expected to produce a solution $\tilde{x}$ of quality higher than any individual x_i^*, as was the case in numerical algorithms presented in this paper.

APPENDIX

A. Generating the Poisson Noise

The Poisson noise is introduced into photon counts y_i as a consequence of limited values of y_i themselves; the lower the total count of the photons, received by a detector per unit of time, the smaller the accuracy of the measurement for the corresponding line integral. The mathematical model of such noise is the Poisson distribution of photon counts: y_i is an instance of the random variable Y_i,

$$Y_i \sim Poisson(\lambda_i), \quad \lambda_i = I_0 e^{-(\mathbf{R}f)_i}. \tag{18}$$

Here f_0 is the scanned image (a 2-D slice of an object), I_0 is the photon count in absence of obstacles (proportional to the initial X-ray intensity), and $(\mathbf{R}f)_i$ is the line integral of the image along the line corresponding to detector i.

In our synthetic experiments, we first compute $\mathbf{R}f$ and then generate the set of photon counts. This is done as follows: **(1)** Denote $g = \mathbf{R}f$ and compute $y_i^0 = I_0 e^{-(g)_i}$ for every bin i in the sinogram. Naturally, the maximal photon count is $\max_i\{y_i^0\} = I_0$ since $min(g) = 0$. The minimal count $y_{min} = \min_i\{y_i^0\}$ depends on the scaling of g. **(2)** We chose this scaling such that $y_{min} = 60$, in order to avoid the problematic numerical behavior related to a low photon count, contaminated with the Poisson noise. Notice that the ratio I_0/y_{min} should be constant when different values of I_0 are used. **(3)** Draw instances of random variables $y_i^n \sim Poisson(y_i^0)$, index i runs over all the bins in the sinogram. **(4)** convert back to the sinogram domain, by computing $g_n = -log(y^n/I_0)$.

B. Statistically-based Iterative Reconstruction

We implement a Penalized-Likelihood reconstruction algorithm, defined in [6] for mono-energetic X-ray scan. Given the noisy measurements y of photon counts, the output image $\tilde{f}$ is computed by minimizing the Penalized Likelihood equation

$$\Psi(f) = L(f|y) + \beta R_\delta(f) \tag{19}$$

where $L(f|y)$ is the negative log-likelihood of the Poisson distribution,

$$L(f|y) = \sum_{i=1}^{N} \{\lambda_i - y_i log(\lambda_i) + log(y_i!)\}, \quad \lambda_i = I_0 e^{-(\mathbf{R}f)_i} \tag{20}$$

and $R_\delta(f)$ is an edge-preserving penalty which encourages image smoothness:

$$R_\delta(f) = \sum_j \{\psi_\delta(\mathbf{D}f)_j\} \tag{21}$$

with $\mathbf{D}f = [\nabla_x f, \nabla_y f]$ consisting of the directional derivative maps of the image f. We compute the derivatives by the central difference approximation. It is defined for x-axis by $f_x(px, py) = f(px + 1, py) - f(px - 1, py)$ and similarly for the y-axis. The Huber penalty ψ_δ is defined by

$$\psi_\delta(x) = \begin{cases} \dfrac{x^2}{2} & \text{if } |x| < \delta, \\ \delta|x| - \dfrac{\delta^2}{2} & \text{if } |x| \geq \delta. \end{cases}$$

The minimizer of equation (19) is computed using a Gradient Descent with a simple line-search function (we did not pursue a computationally effective implementation, since only the quality of the algorithm output is considered). The parameters β, δ and the number of iterations were tuned on the training images for each image to attain the best possible SNR value.

REFERENCES

[1] G. N. Ramachandran and A. V. Lakshminarayanan, "Three-dimensional Reconstruction from Radiographs and Electron Micrographs: Application of Convolutions instead of Fourier Transforms," *Proceedings of the National Academy of Sciences of the United States of America*, vol. 68, no. 9, pp. 2236–2240.

[2] K.I. Kim J.H. Kim and C.E. Kwark, "A filter design for optimization of lesion detection in spect," *IEEE Nuclear Science Symposium*, vol. 3, pp. 1683–1687, 1996.

[3] T. Olson and J. DeStefano, "Wavelet localization of the radon transform," *IEEE Trans Signal Process.*, vol. 42, no. 8, pp. 2055–2067, Aug. 1994.

[4] A.H. Delaney and Y. Bresler, "Multiresolution tomographic reconstruction using wavelets," *IEEE Trans. on Image Processing*, vol. 4, no. 6, pp. 799 – 813, Jun. 1995.

[5] C.A. Berenstein F. Rashid-Farrokhi, K.J. Ray Liu and D. Walnut, "Wavelet-based multiresolution local tomography," *IEEE Trans. Med. Imag.*, vol. 6, no. 10, pp. 1412–1430, Oct. 1997.

[6] I.A. Elbakri and J.A. Fessler, "Statistical image reconstruction for polyenergetic x-ray computed tomography," *IEEE Trans. Med. Imag.*, vol. 21, no. 2, pp. 89–99, Feb. 2002.

[7] J.A. Fessler, "Iterative methods for image reconstruction," in *IEEE International Symposium on Biomedical Imaging*.

[8] K.D. Sauer B.I. Andia and C.A. Bouman, "Nonlinear backprojection for tomographic reconstruction," *IEEE Trans Nucl Sci*, vol. 49, no. 1, pp. 61–68, Feb. 2002.

[9] M. Zibulevsky J. Shtok, M. Elad, "Adaptive filtered-back-projection for computed tomography," in *IEEE 25-Th Convention Of Electrical And Electronics Engineers In Israel*. Mar. 2008, pp. 528–532, IEEE.

[10] M. Zibulevsky J. Shtok, M. Elad, "Direct adaptive reconstruction algorithms for computed tomography," in *IEEE International Symposium on Biomedical Imaging: From Nano to Macro*, 2009.

[11] A. Goldenshluger and A. Nemirovsky, "On spatial adaptive estimation of nonparametric regression," *Math. Meth. Statist.*, vol. 6, no. 2, pp. 135–170, 1997.

[12] J. Bian P.J. La Rivire and P.A. Vargas, "Penalized-likelihood sinogram restoration for computed tomography," *IEEE Trans. Med. Imag.*, vol. 25, no. 8, pp. 1022–36, Aug. 2006.

[13] V.G. Spokoiny O.V. Lepskii, E. Mammen, "Optimal spatial adaptation to inhomogeneous smoothness: An approach based on kernel estimates with variable bandwidth selectors," *Ann. Statist.*, vol. 25, no. 3, pp. 929–947, 1997.

[14] O.V. Lepski, "One problem of adaptive estimation in gaussian white noise," *Theory Probab. Appl.*, vol. 35, no. 3, pp. 459–470, 1990.

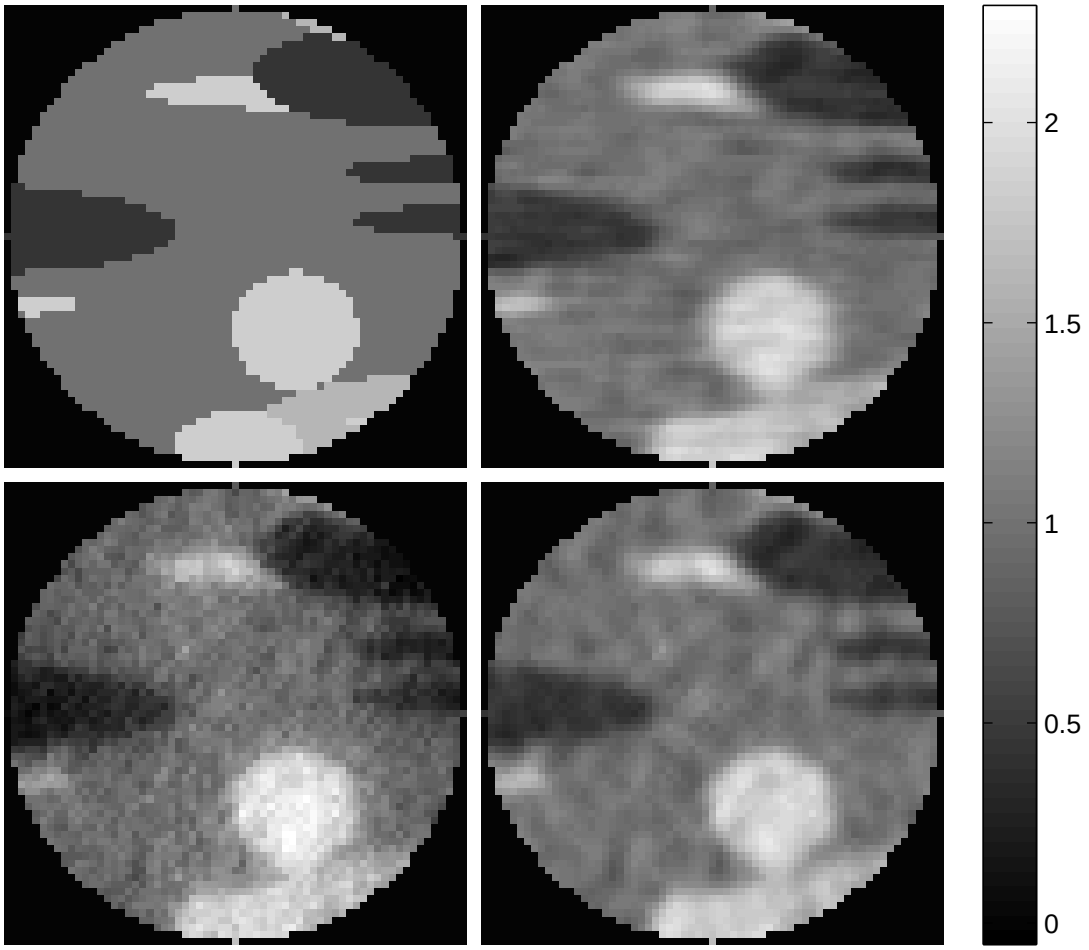
2
1.5
1
0.5
0